Control of a battery energy storage system to compensate for ADN equivalents inaccuracies

Gilles Chaspierre
Dept. of Elec. Eng. and Comp. Science
University of Liège, Belgium
gilles.chaspierre@kuleuven.be

Patrick Panciatici
Research & Development Dept.
RTE, Versailles, France
patrick.panciatici@rte-france.com

Thierry Van Cutsem
Fund for Scientific Research (FNRS)
University of Liège, Belgium
t.vancutsem@uliege.be

***Abstract*—This paper proposes a new application for a Battery Energy Storage System (BESS) connected at distribution level. It consists of controlling the BESS in such a way that the net active and reactive powers entering the distribution network matches as closely as possible the response of a dynamic equivalent model of the latter, used in large-disturbance dynamic simulations of the transmission system. Thus, the BESS compensates for the inevitable inaccuracies of the equivalent, which can be used with higher guarantee of accuracy. The battery is supposed to be available for other purposes at the main substation of the distribution grid. Its active and reactive powers are controlled without resorting to any model of that grid. Simulations results are reported on the CIGRE MV test system. Good performances are found in response to disturbances of various severities.**

***Index Terms*—Active distribution network, Battery energy storage system, Dynamic equivalent, Inverter-based generator**

I. Introduction

With the growing presence of Inverter-Based Generators (IBG) connected at distribution level, the modelling of active distribution networks (ADNs) shows up more and more challenging. Recent works have been devoted to deriving reduced-order dynamic models of ADNs that can be used by Transmission System Operators (TSOs) in dynamic simulations of their systems subject to large disturbances (e.g. [1]–[5]). The focus in this paper is on "grey-box" equivalents. Since large disturbances are of concern, measured system responses are scarce, and a simulation-based approach is used to optimally adjust the parameters of the equivalent.

However, as emphasized in [1], [2], ADN models are affected by uncertainty, which leads to inevitable discrepancies between the response of the equivalent and that of the real ADN. This paper explores a new approach to this problem. It takes advantage of the growing use of BESS at distribution level. Indeed, the BESS technology is constantly evolving and several applications to ADNs have become a reality, such as primary frequency control provision [6], flexible power management [7] or participation in voltage regulation [8]. One step further, Ref. [9] proposes a real-time control of a BESS for concurrent primary frequency and local voltage regulation.

The idea developped in this paper can be summarized as follows. In the event of a large disturbance in the transmission system, the BESS is controlled in such a way that the power entering the distribution grid follows the equivalent ADN model as closely as possible. The outcome is that the equivalent can be used in dynamic simulations of the transmission system with higher guarantee of accuracy. Since the BESS is called to respond to infrequent large disturbances and over short periods of time, the energy used is small. Yet, to minimize the use of the battery for this particular application, it is in the interest of the DSO that the best possible equivalent is used. In other words, the BESS would increase the reliability of the equivalent model, with an incentive to improve the quality of the latter to minimize the use of the battery.

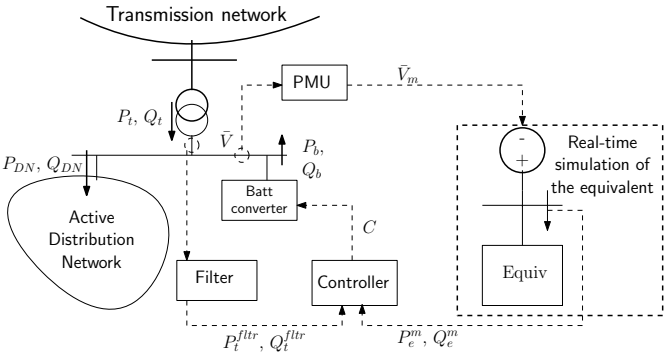

Fig. 1: Overall configuration of the proposed BESS control

With this new application, the parameters of the equivalent could be updated less frequently (in response to distribution network evolutions or changing operating conditions), since the BESS would be able to compensate for the inaccuracies of the equivalent with respect to the real system behaviour (which in any case is not known exactly). Of course, because of its limited capacity, there will be some point where the BESS will no longer be able to compensate for the inaccuracies of the equivalent, and the latter must be updated in order the BESS to provide the expected service.

The overall configuration is sketched in Fig. 1. The active and reactive powers (P_t, Q_t) flowing out of the distribution transformer are measured, as well as the voltage phasor $\bar{V} = Ve^{j\delta}$ at its Medium Voltage (MV) bus. P_t^{fltr} and Q_t^{fltr} are the active and reactive power output of a filter accounting for measurements delay and smoothing. In response to a disturbance in the transmission system (detected by a significant change in V), the response of the equivalent is simulated in real time using the measured MV voltage phasor $\bar{V}_m$. A Phasor Measurement Unit (PMU) is needed for that purpose since

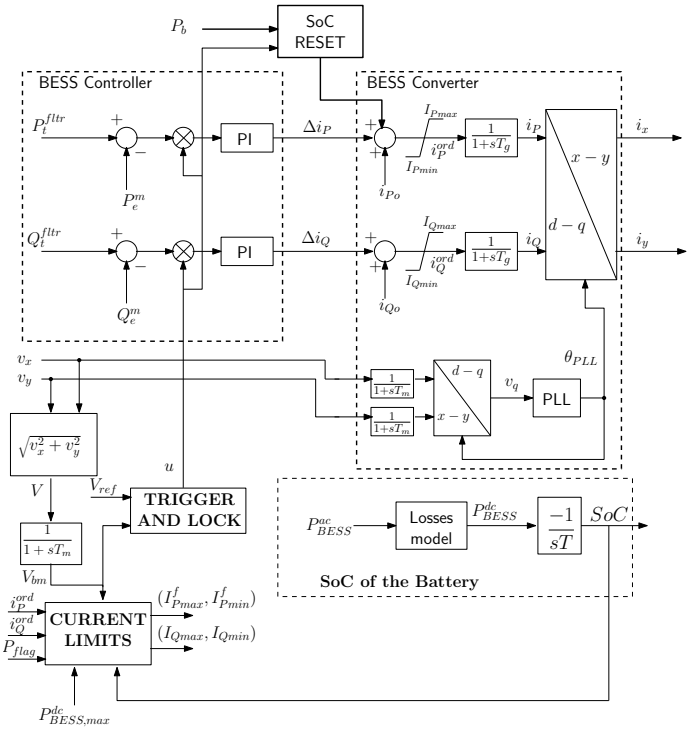

Fig. 2: Model of the BESS controller and converter

it is required to account for the change in both magnitude and phase angle of the voltage to accurately simulate the response of the equivalent. The simulated powers P_e^m and Q_e^m along with the measured powers P_t^{fltr} and Q_t^{fltr} are used to control the BESS active P_b (resp. reactive Q_b) power to satisfy $P_t^{fltr} \approx P_e^m$ and $Q_t^{fltr} \approx Q_e^m$. The controller takes into account the maximum current of the converter and other limits. Note that it does not use any model of the ADN.

The rest of the paper is organized as follows. Section II details the BESS controller and converter models. The set up of the simulations is outlined in Section III. Simulation results on a variant of the CIGRE MV test system [10] are presented in Section IV. A summary and concluding remarks are offered in Section V.

II. Modelling the BESS, its converter and its controller

The model of the BESS converter is presented in block-diagram form in Fig. 2. The DC part of the DC/AC converter is not modeled since it is not relevant for the range of dynamics considered here [11]. Instead, the DC voltage is assumed to remain constant. This allows the converter to independently control the active and reactive powers [12].

The inputs v_x and v_y are the projections of the phasor of the BESS terminal voltage on the rotating reference axes (x, y) used in phasor-mode simulation [13]. The outputs i_x and i_y are the corresponding projections of the phasor of the current injected by the BESS.

The time constant T_m accounts for the voltage magnitude measurement delay, while T_g is the time constant of the converter current regulator [14]. i_P^o (resp. i_Q^o) is the initial value of the active (resp. reactive) current, before the disturbance occurrence. The dynamics of the fast electronic components are not considered.

Figure 2 also shows the BESS controller. It simply consists of two Proportional-Integral (PI) controllers, one for the active power and the other for the reactive power. Their outputs Δi_P and Δi_Q (corresponding to C in Fig. 1) are corrections added to i_P^o and i_Q^o to obtain the current orders i_p^{ord} and i_Q^{ord}.

A. Phase-Locked Loop (PLL)

The PLL provides an estimate θ_{PLL} of the terminal voltage phase angle. This is needed to give to the injected current the proper phase angle with respect to that voltage. The PLL model is generic but allows to account for a nonzero response time. It is the same model as the one presented in [15].

B. Current limits

While controlling the active and reactive powers, the output current must not exceed the converter limit I_{nom}. To this purpose the active and reactive currents are upper limited to:

$$I_{Pmax} = P_{flag} I_{nom} + (1 - P_{flag}) \sqrt{I_{nom}^2 - (i_Q^{ord})^2} \quad (1)$$

$$I_{Qmax} = P_{flag} \sqrt{I_{nom}^2 - (i_P^{ord})^2} + (1 - P_{flag}) I_{nom} \quad (2)$$

respectively, where P_{flag} is a binary parameter that gives priority to either the active or the reactive current. In the former case, P_{flag} = 1, while in the latter case, P_{flag} = 0.

Since the BESS powers can flow in both directions, the active and reactive currents are lower limited symmetrically, i.e.:

$$I_{Pmin} = -I_{Pmax} \qquad I_{Qmin} = -I_{Qmax}. \quad (3)$$

In addition to the converter current, the power P_{BESS}^{dc} delivered by the battery is also limited according to [6]:

$$P_{BESS}^{dc} \leq P_{BESS,max}^{dc} \quad (4)$$

where P_{BESS}^{dc} is the sum of the converter active power output and internal losses:

$$P_{BESS}^{dc} = P_{BESS}^{ac} + P^{loss} = P_{BESS}^{ac} + (1 - \eta) \sqrt{P_{BESS}^{ac2} + Q_{BESS}^{ac2}} \quad (5)$$

with η being the converter efficiency. In a first approximation, an ideal converter ($\eta = 1$) is assumed, which yields:

$$i_P = \frac{P_{BESS}^{ac}}{V_{bm}} \simeq \frac{P_{BESS}^{dc}}{V_{bm}} \quad (6)$$

and the limits finally applied to the active current are:

$$I_{Pmax}^f = min(I_{Pmax}, \frac{P_{BESS,max}^{dc}}{V_{bm}}) \quad (7)$$

$$I_{Pmin}^f = max(I_{Pmin}, -\frac{P_{BESS,max}^{dc}}{V_{bm}}) \quad (8)$$

where V_{bm} is the voltage magnitude measured by the BESS (see Fig. 2).

C. Battery state of charge

The State of Charge (SoC) of the battery is explicitly represented as shown in Fig. 2. P^{dc}_{BESS} is the power delivered by the battery, the time constant T is the rated maximum charging/discharging time.

This part of the model may also affect the value of I_{pmin} if $SoC > SoC_{max}$ (resp. the value of I_{Pmax} if $SoC < SoC_{min}$). When the SoC reaches one of its limits, the bound I^f_{Pmax} or I^f_{Pmin} in (7, 8) is set to zero. This is integrated in the CURRENT LIMITS block in Fig. 2, which receives SoC as an input. SoC_{min} and SoC_{max} are set to typical values, i.e. 20 % and 80 %, respectively [11].

D. Resetting the SoC of the BESS

Using the BESS to approach the dynamic response of an equivalent model should not affect the other services it is expected to provide, such as power balancing, contribution to frequency control, etc. [6], [7]. Furthermore, the BESS should be prepared to face the next disturbance.

Therefore, once the system has settled to (quasi-)steady state, it is desirable to restore the SoC of the BESS to its pre-disturbance value. This reset must be smooth to avoid disturbing the ADN and, to some extent, the transmission system. One option is to have the SoC restored before the load tap changer starts acting on the distribution transformer ratio, in order to avoid interactions with that device.

This action is carried out by a separate controller that computes the variation of the energy stored in the BESS due to its dynamic contribution (P_b), i.e. :

$$\Delta E(t) = \int_{t_{dis}}^{t} \left(P_b(\tau) - P_b(t_{dis})\right) d\tau \tag{9}$$

where t_{dis} is the time of the disturbance occurrence. To slowly steer ΔE back to zero (and, hence, restore the SoC), an integral controller uses ΔE as input and adds its output to the active current order i^{ord}_P, as shown in Fig. 2). At the same time, u is reset to zero to disable the BESS control based on power flows.

E. Control triggering and locking

To avoid undesired repeated solicitations, the BESS should not react to the small voltage variations that accompany load changes, maneuvers, generator voltage adjustments, transformer tap changes, etc. On the contrary, it reacts to more severe disturbances in the transmission grid, such as faults, which are detected through significant variations of V_{bm}.

To this purpose, the TRIGGER AND LOCK block in Fig. 2: (i) keeps the controller idle as long as V_{bm} remains in a deadband $[V_{ref} - \epsilon \;\; V_{ref} + \epsilon]$ where V_{ref} is a reference voltage and ϵ a tolerance; (ii) triggers the control as soon as V_{bm} leaves the deadband and (iii) keeps the controller active, whatever the subsequent voltage evolution, until it is reset as previously described.

The output u of the block is a binary variable with value 0 when the controller is idle, and 1 when it is active. Through the multipliers (see Fig. 2), $u = 0$ forces the inputs of the PI controllers to zero and hence $\Delta i_P = \Delta i_Q = 0$.

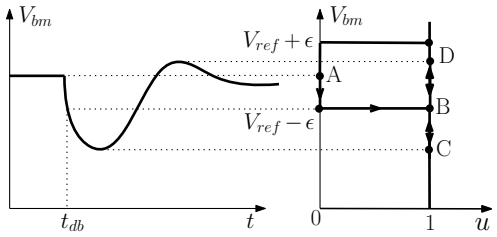

Fig. 3: TRIGGER AND LOCK block of the BESS controller

The above features are modelled with the hysteresis block shown in Fig. 3. The right diagram shows how u changes for the voltage evolution shown in the left plot. The initial voltage is inside the deadband; the corresponding operating point is A. The voltage leaves the deadband at time t_{db}, causing u to change from 0 to 1 (point B), at which it remains locked. The minimum and maximum voltage deviations correspond to points C and D, respectively. A similar transition takes place if $V_{bm} > V_{ref} + \epsilon$.

III. SET UP OF THE SIMULATIONS

A. Voltage phasor measurement process

Taking into account the voltage measurement process by a Phasor Measurement Unit (PMU) is somewhat delicate. Indeed, the model is to be used in large-disturbance simulations. While a PMU is a highly accurate power system instrument, its accuracy is considerably impacted by the errors in instrumentation channels (instrument transformers, control cables, attenuators, etc.) and system imbalances [16]. Accuracy is further deteriorated in dynamic conditions (in particular if power-electronics interfaced devices are involved) [16]. Furthermore, as outlined in the next section, simulations are performed under the phasor approximation. Faithful simulations of a PMU signal processing algorithm should rely on electromagnetic transients simulations of the voltage "wave".

Having in mind that the focus here is on demonstrating the concept of BESS control, a simple model of the voltage phasor measurement process (block PMU in Fig. 1) was adopted. It accounts for the smoothing of the PMU outputs aimed at avoiding outlier phasors during transients. A weighted moving average filter is applied to $\bar{V} = v_x + jv_y$ to produce the filtered voltage phasor:

$$\bar{V}_m = V_m \angle \delta_m = \sum_{i=0}^{N-1} w_i \left[v_x(t - i\Delta t) + jv_y(t - i\Delta t)\right] \tag{10}$$

where N is the time window length and w_i the weight assigned to the i-th sample. Both N and the w_i's were tuned to reduce measurement delays without deteriorating noise rejection. More details and examples of performance can be found in [17] (Appendix D).

B. Phasor-mode simulation

Simulations were performed with the phasor-mode time-domain simulation software RAMSES, whose solver is detailed in [18]. Due to the presence of small delays, the time step size used to integrate the differential-algebraic equations was set to the low value of 1 ms.

Both the full (unreduced) ADN and its (reduced-order) equivalent are simulated in parallel. The simulation of the equivalent mimics a real-time simulator whose purpose is to generate the P_e^m and Q_e^m values (see Fig. 1). This real-time simulator is assumed to have a negligible computing time, so that no associated delay is considered. This is acceptable considering the small size of the equivalent model.

A separate "discrete controller" implements the weighted moving-average filter of Eq. (10). The term discrete controller refers to a piece of code that is executed at the end of each time step. It updates the value of the voltage phasor $\bar{V}_m$ every 5 ms.

The BESS controller is also simulated through a discrete controller that updates the Δi_P and Δi_Q commands every 5 ms. To that purpose, the PI controller equations are implemented in discrete-time form.

IV. Simulation Results

A. Test system and its equivalent

The simulations were perfomed on a variant of the CIGRE MV Distribution Network Benchmark [10]. Its one-line diagram is shown in the left part of Fig. 4. A BESS (shown in red) has been connected to the main substation.

The model includes static and motor loads as well as IBGs. The large-capacity IBGs have low-voltage ride-through and reactive current injection capabilities, while the small residential IBGs have not and disconnect if their terminal voltage falls below 0.8 pu.

The uncertainty affecting the parameters of the model was assessed as detailed in [1], [2], [17]. Monte-Carlo (MC) simulations involving randomized values of the parameters were carried out, from which the time-varying averages and variances of the active (resp. reactive) power P_{DN} (resp. Q_{DN}) (see Fig. 1) were extracted.

The ADN equivalent is shown in the right part of Fig. 4. Its components and the identification of its parameters were detailed in [1], [2], [17]. It was tuned to approach the average response of the ADN, obtained from the MC simulations. Note that the equivalent accounts for the disconnection of residential IBGs in low voltage conditions.

To deal with a case where the BESS is expected to significantly compensate for the inaccuracy of the equivalent, a parameter set was selected yielding a response of the unreduced ADN model rather "far" from the average evolution used to tune the equivalent.

B. Parameters of the BESS converter and controller

The filter with inputs P_t and Q_t and outputs P_t^{fltr} and Q_t^{fltr} (see Fig. 1) has been modelled by a first-order transfer function with a time constant T_{fltr} of 10 ms.

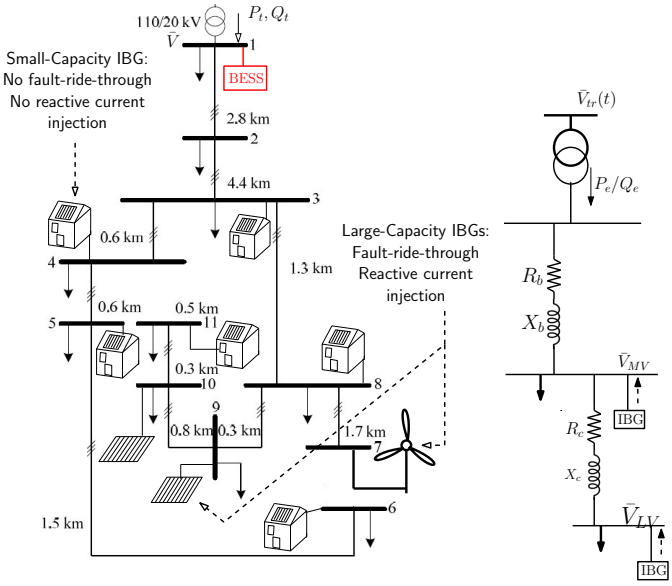

Fig. 4: Modified CIGRE MV Distribution Network Benchmark: unreduced ADN (left) and its equivalent (right)

In pre-disturbance conditions, the BESS produces $P_b(0) = 2$ MW and $Q_b(0) = 1$ Mvar. This may account for other services that the BESS is providing. It leads to nonzero i_{Po} and i_{Qo} values (see Fig. 2), which are assumed to remain constant throughout the simulation.

The time constant T_g of the BESS converter (see Fig. 2) has been set to 20 ms. The parameters of the BESS PI controllers (see Fig. 2) have been adjusted to achieve good performances in response to multiple disturbances. As regards the model in Fig. 3, ϵ has been set to 0.05 pu and V_{ref} to 1 pu. The deadband is thus $[0.95\ 1.05]$ pu.

C. Simulation of a voltage dip followed by a phase jump

The performance of the BESS control is assessed in response to a voltage dip of 0.8 pu lasting for 100 ms, followed by a voltage phase jump of -10 deg. Both are applied to the voltage on the transmission side of the transformer. Furthermore, the post-disturbance voltage magnitude is slightly lower than its pre-disturbance value. This sequence is representative of a short-circuit in the transmission grid, cleared by normal protections opening a loaded transmission line.

The evolutions of, respectively, the voltage magnitudes V and V_m and the phase angles δ and δ_m are shown in Fig. 5. As desired, the model of the voltage phasor measurement process (see Section III) introduces a small delay, after which the magnitude and phase angle are accurately tracked. At $t = 0.1$ s, when the voltage magnitude drops, δ starts decreasing, while when the magnitude recovers, at $t = 0.2$ s, the reverse evolution of δ is canceled by the imposed phase jump of -10 deg, resulting in a further decrease of 4 deg.

The voltage dip triggers and locks the BESS controller, as explained in Section II-E.

The evolution of the active power, without and with BESS control, as well as the active power delivered by the BESS are

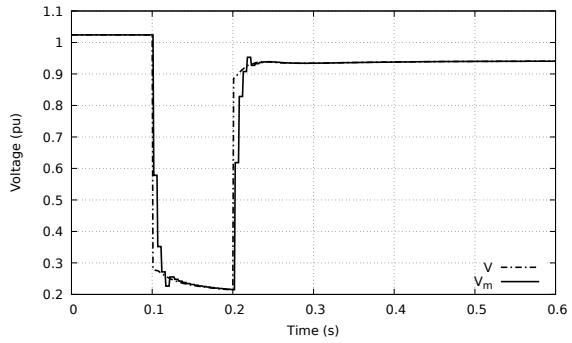

(a) V vs. V_m

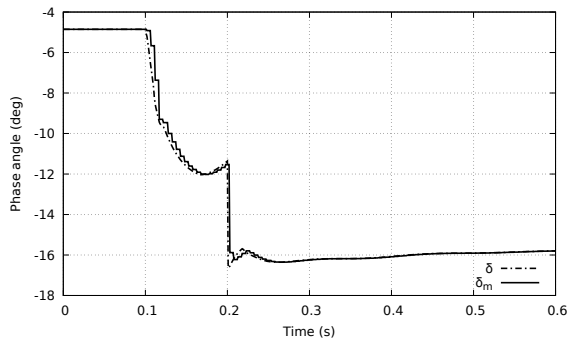

(b) δ vs. δ_m

Fig. 5: Voltage dip followed by phase jump: evolution of: (a) V and V_m, (b) δ and δ_m

shown in Figs. 6a to 6c. Figure 6a compares the evolutions of P_e and P_t in the absence of the proposed BESS control. It is recalled that P_t is the power entering the real ADN (see Fig. 1), whose model is not known accurately. P_e is the corresponding power flow in the equivalent, which would be used by the TSO in its dynamic simulations. The figure shows that the evolution of P_t does not well match that of P_e. On the other hand, when the BESS controller is active, P_t is much closer to P_e, as can be seen in Fig. 6b. The active power P_b produced by the BESS is shown in Fig. 6c. It is observed that the BESS generates active power oscillations to compensate for the oscillatory discrepancies between P_e and P_t.

The evolution of P_t^{fltr} and P_e^m are shown in Fig. 6d. Both powers are identified in Fig. 1. P_e^m is the power entering the ADN, determined by the real-time simulation of the ADN equivalent; it includes the delay induced by the filter (10). The BESS is controlled to bring $|P_t^{fltr} - P_e^m|$ to zero.

Similar observations are made on the reactive powers. The evolutions of Q_t and Q_e, respectively without and with the BESS contoller are shown in Fig. 7. The proposed control brings Q_t significantly closer to Q_e, thereby making the equivalent more accurate.

D. An indicator of accuracy of the equivalent

In this section, two instances of the ADN model differing by the values of its parameters are considered. The first one, denoted by ADN A, shows up a power response close to that of the equivalent. The second one, denoted ADN B, has been

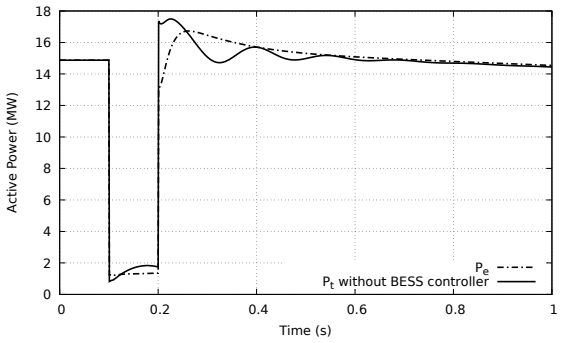

(a) P_t vs. P_e without BESS controller

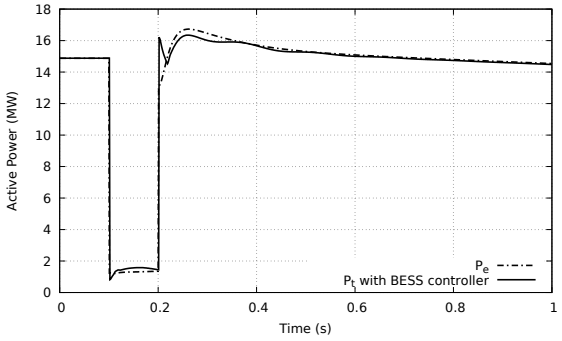

(b) P_t vs. P_e with BESS controller

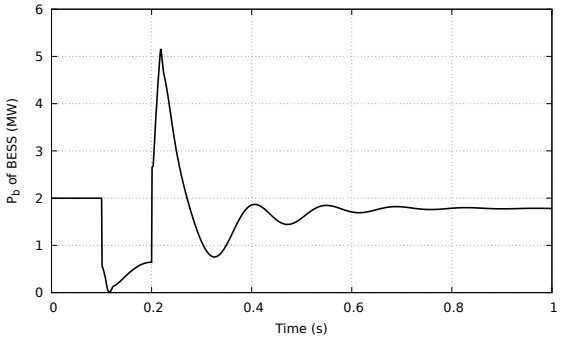

(c) Active power P_b produced by the BESS

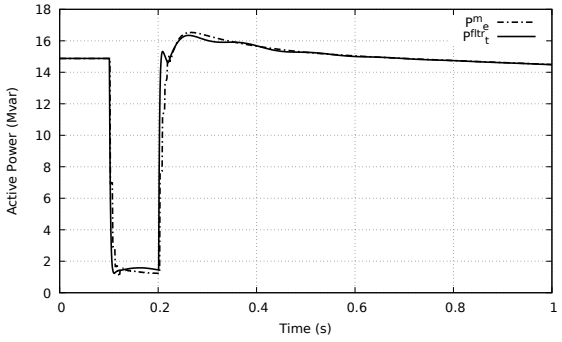

(d) P_t^{fltr} vs. P_e^m

Fig. 6: Evolutions of active powers

considered in the previous section. Thus, in the former case the equivalent is accurate while in the latter case it is less.

A severe voltage dip is now considered, in which the transmission voltage drops by 0.7 pu for 250 ms before

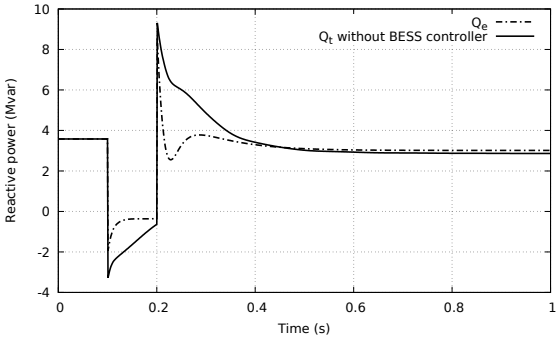

(a) Q_t vs. Q_e without BESS controller

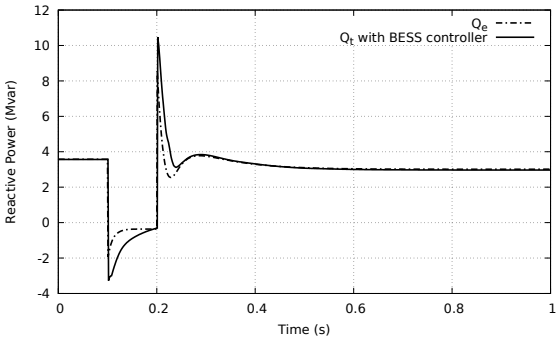

(b) Q_t vs. Q_e with BESS controller

Fig. 7: Evolution of reactive powers

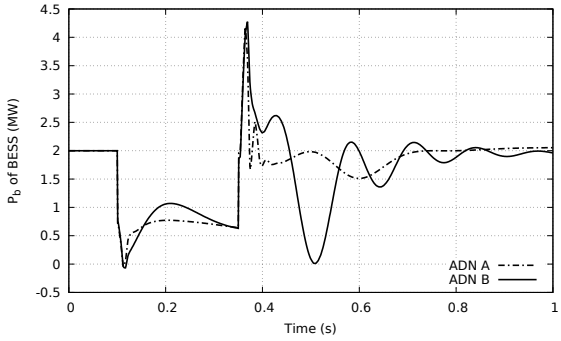

Fig. 8: Active power

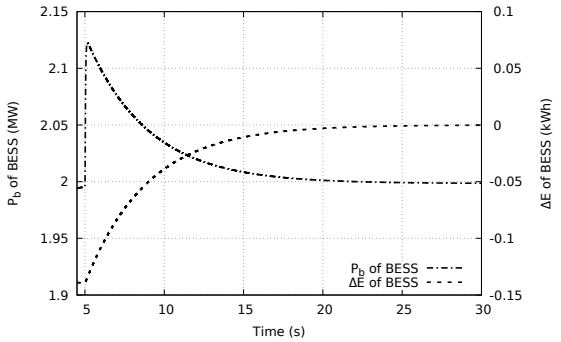

Fig. 9: Restoring the SoC: active power and variation of energy

recovering its pre-fault value.

Figure 8 shows the active power produced by the BESS dealing with ADN A and ADN B, respectively. Expectedly, the variation of active power (with respect to $P_b(0)$) is larger for ADN B.

The latter variation can be used in an indicator of accuracy of the equivalent with respect to the real system (whose exact model is not known). This indicator of accuracy is computed as:

$$\varepsilon_P = \sqrt{\frac{1}{t_{fin} - t_{act}} \int_{t_{act}}^{t_{fin}} \left(P_b(\tau) - P_b(t_{act})\right)^2 d\tau} \qquad (11)$$

where t_{act} is the time when the BESS contribution is activated and t_{fin} the time when the BESS returns to steady state. ε_P is expressed in MW.

If, for a given disturbance, ε_P exceeds some threshold, it is an indication that the equivalent should be updated. This is in the interest of both the DSO and the TSO. The former avoids an excessive contribution of the battery while the latter benefits from a more reliable ADN model.

In the example of Fig. 8, considering that $t_{act} = 0.1$ s and $t_{fin} = 1.1$ s, the value of ε_P is 0.69 MW for ADN A and 0.81 MW for ADN B. This represents a 17.4 % increase of the battery contribution when the distribution system obeys the model given by ADN B, for which the equivalent is less accurate.

ε_P reflects the accuracy of the equivalent in terms of active power response. A similar indicator is obtained for reactive power by substituting Q_b to P_b in Eq. (11).

E. Restoring of the BESS SoC

As explained in Section II-D the BESS reset is aimed at steering ΔE back to zero when the transients have died out.

The corresponding simulation results are shown in Fig. 9. They relate to ADN B and the severe voltage dip of Section IV-D. At time $t = 5$ s, when power flows P_t and Q_t have reached steady values, the reset process starts. ΔE increases progressively and reaches zero after 20 s. Figure 9 also shows the evolution of P_b. In the specific scenario, P_b must be increased to restore the SoC of the BESS.

F. BESS response with current limit

In the previous simulations, the BESS current was not limited. To activate the limitation, the nominal apparent power of the BESS has been reduced to 5 MVA. The results hereafter relate to ADN B and the severe voltage dip of Section IV-D.

Figure 10a shows the evolution of P_e (the reference) and P_t for three settings of the BESS controller: current limit ignored, priority to active current and priority to reactive current, respectively. The plots zoom on the time interval immediately after voltage recovery. The corresponding results for reactive power are shown in Fig. 10b.

In this scenario, the active power response is little impacted by the choice of priority. This is due to the fact that the correction Δi_P is small at the time the upper bound I_{Pmax} is decreased according to Eq. (1) (where $Pflag = 0$). The

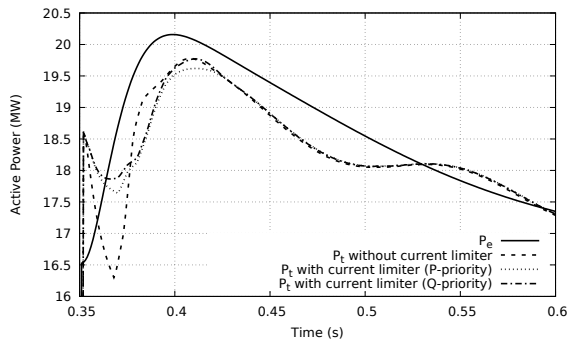

(a) Active power

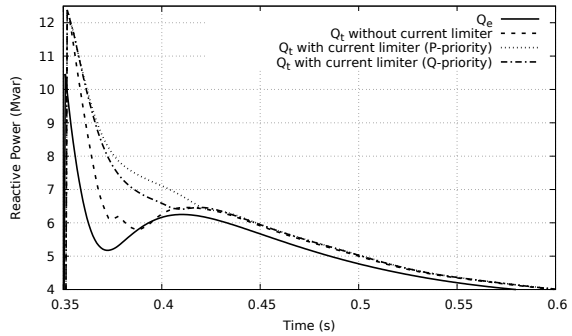

(b) Reactive power

Fig. 10: Evolution of BESS powers when current gets limited

reactive power is more noticeably impacted and, as expected, Q_t gets closer to Q_e when priority is given to reactive current.

Figure 10a shows a paradox: the discrepancy between P_e and P_t is larger without than with current limit. This is due to the delay between P_t^{fltr} and P_e^m at voltage recovery, leading to an undesirable large correction Δi_P, avoided when current limits are taken into account.

V. Conclusion

A new application has been proposed for a BESS connected to a distribution grid. It consists in controlling its active and reactive powers so that, after a large enough disturbance, the net power entering the distribution grid evolves with the distribution voltage as closely as possible to the response provided by an equivalent.

The latter is a reduced-order model used in simulations of the transmission system. The overall objective is to compensate for inevitable inaccuracies of that model and, hence, increase the reliability of those simulations.

The BESS control involves the measurement of the distribution voltage phasor, a real-time simulation of the equivalent response, PI controllers adjusting the BESS active and reactive current orders, current limiters obeying either active or reactive power priority, and a slow energy reset control. The BESS does not react to voltage variations below some threshold.

Simulation results show good performance of the proposed control, while accounting for delays in the control loop.

By compensating for the inaccuracies of the equivalent, the proposed control allows less frequent updates of the latter. Nevertheless, an indicator of accuracy is available to point out situations where the equivalent should be updated, thereby avoiding excessive use of the BESS.

Further developments of the proposed concept should rely on electromagnetic transients simulations and hardware-in-the-loop tests.

References

[1] G. Chaspierre, G. Denis, P. Panciatici, and T. Van Cutsem, "Dynamic equivalent of an active distribution network taking into account model uncertainties," *Proc. 13th IEEE PES PowerTech conference*, Milan (Italy), 2019.

[2] ——, "An active distribution network equivalent derived from large-disturbance simulations with uncertainty," *IEEE Transactions on Smart Grid*, vol. 11, no. 6, pp. 4749–4759, 2020.

[3] F. Conte, F. D'Agostino and F. Silvestro, "Operational constrained nonlinear modeling and identification of active distribution networks," *Electric Power Systems Research*, vol. 168, pp. 92–104, 2019.

[4] X. Shang, Z. Li, J. Zheng and Q.H. Wu, "Equivalent modeling of active distribution network considering the spatial uncertainty of renewable energy resources," *International Journal of Electrical Power and Energy Systems*, vol. 112, pp. 83–91, 2019.

[5] N. Fulgêncioa, C. Moreira, L. Carvalho and J. P. Lopes, "Aggregated dynamic model of active distribution networks for large voltage disturbances," *Electric Power Systems Research*, vol. 178, pp. 1–13, 2019.

[6] G. P. Schiapparelli, S. Massucco, E. Namor, F. Sossan, R. Cherkaoui, and M. Paolone, "Quantification of primary frequency control provision from battery energy storage systems connected to active distribution networks," *2018 Power Systems Computation Conference (PSCC)*, pp. 1–7, 2018.

[7] N. Karthikeyan, B. R. Pokhrel, J. R. Pillai, and B. Bak-Jensen, "Utilization of battery storage for flexible power management in active distribution networks," *2018 IEEE Power & Energy Society General Meeting (PESGM)*, pp. 1–5, 2018.

[8] M. Zeraati, M. E. H. Golshan, and J. M. Guerrero, "A consensus-based cooperative control of pev battery and pv active power curtailment for voltage regulation in distribution networks," *IEEE Transactions on Smart Grid*, vol. 10, no. 1, pp. 670–680, 2017.

[9] A. Zecchino, Z. Yuan, F. Sossan, R. Cherkaoui, and M. Paolone, "Optimal provision of concurrent primary frequency and local voltage control from a bess considering variable capability curves: Modelling and experimental assessment," *Proc. 21th PSCC conf.*, Porto (Portugal), 2020.

[10] S. Barsali *et al.*, *Benchmark systems for network integration of renewable and distributed energy resources*. CIGRE Task Force, 2014.

[11] "WECC Battery Storage Dynamic Modeling Guideline," November, 2016.

[12] A. Jalali, M. G. Dozein, and P. Mancarella, "Frequency Stability Provision From Battery Energy Storage System Considering Cascading Failure s with Applications to Separation Events in Australia," *Proc. 13th IEEE PES PowerTech conference*, Milan (Italy), 2019.

[13] P. Kundur, *Power system stability and control*. McGraw-hill New York, 1994.

[14] Western Electricity Coordinating Council Modeling and Validation Work Group, "WECC Solar Plant Dynamic Modeling Guidelines," *WECC Renewable Energy Modeling Task Force*, May 2014.

[15] G. Chaspierre, P. Panciatici and T. Van Cutsem, "Aggregated Dynamic Equivalent of a Distribution System hosting Inverter-based Generators," *Proc. 20th PSCC conference*, Dublin (Ireland), 2018.

[16] Z. Huang, B. Kasztenny, V. Madani, K. Martin, S. Meliopoulos, D. Novosel, and J. Stenbakken, "Performance evaluation of phasor measurement systems," in *2008 IEEE Power and Energy Society General Meeting-Conversion and Delivery of Electrical Energy in the 21st Century*. IEEE, 2008, pp. 1–7.

[17] G. Chaspierre, "Reduced-order modelling of active distribution networks for large-disturbance simulations," Ph.D. dissertation, University of Liège (Belgium), October, 2020. [Online]. Available: http://hdl.handle.net/2268/251602

[18] P. Aristidou, D. Fabozzi and T. Van Cutsem, "Dynamic simulation of large-scale power systems using a parallel Schur-complement-based decomposition method," *IEEE Trans. on Parallel and Distributed Systems*, vol. 25, no. 10, pp. 2561—-2570, 2014.